Title

Internal Heat Transfer Coefficient Determination in a Packed Bed From the Transient Response Due to Solid Phase Induction Heating

Journal

Journal of Heat Transfer, 134(4)

ISSN

00221481

Authors

Geb, David
Zhou, Feng
Catton, Ivan

Publication Date

2012

DOI

10.1115/1.4005098

Peer reviewed

Internal Heat Transfer Coefficient Determination in a Packed Bed From the Transient Response Due to Solid Phase Induction Heating

David Geb[1]
e-mail: dvdgb15@ucla.edu

Feng Zhou

Ivan Catton

Morrin-Gier-Martinelli Heat Transfer Memorial Laboratory,
Department of Mechanical and Aerospace Engineering,
School of Engineering and Applied Science,
University of California,
Los Angeles,
48-121 Engineering IV, 420 Westwood Plaza,
Los Angeles, CA 90095-1597

Nonintrusive measurements of the internal heat transfer coefficient in the core of a randomly packed bed of uniform spherical particles are made. Under steady, fully-developed flow the spherical particles are subjected to a step-change in volumetric heat generation rate via induction heating. The fluid temperature response is measured. The internal heat transfer coefficient is determined by comparing the results of a numerical simulation based on volume averaging theory (VAT) with the experimental results. The only information needed is the basic material and geometric properties, the flow rate, and the fluid temperature response data. The computational procedure alleviates the need for solid and fluid phase temperature measurements within the porous medium. The internal heat transfer coefficient is determined in the core of a packed bed, and expressed in terms of the Nusselt number, over a Reynolds number range of 20 to 500. The Nusselt number and Reynolds number are based on the VAT scale hydraulic diameter, $d_h = 4\varepsilon/S$. The results compare favorably to those of other researchers and are seen to be independent of particle diameter. The success of this method, in determining the internal heat transfer coefficient in the core of a randomly packed bed of uniform spheres, suggests that it can be used to determine the internal heat transfer coefficient in other porous media.
[DOI: 10.1115/1.4005098]

Keywords: packed bed, porous media, internal heat transfer coefficient, volume averaging theory, two-temperature model, single-blow transient technique, induction heating, bypass effect, channeling effect

Introduction

Determining the heat transfer coefficient in a porous medium experimentally is challenging primarily due to its complicated geometry. Transient test methods are often applied to determine the heat transfer characteristics of complicated surfaces, such as that found in packed particle beds, due to their relative ease and cost effectiveness when compared to steady state methods such as those described by Kays and London [1,2]. In the literature on the subject, many transient test methods are often described as "single-blow" transient test techniques. In such single-blow tests, a single fluid stream, under steady flow conditions, is subjected to an inlet fluid temperature perturbation. The temperature perturbation could be a step-change or an oscillatory function. The inlet and outlet stream temperatures are measured continuously over an interval of time and compared to the predictions of a model in order to determine the desired heat transfer information. This single-blow method, and its variations, along with various other transient techniques have been investigated since the 1920 s.

Hausen [3], Schumann [4], Locke [5], and Kohlmayer [6,7] performed much of the crucial early work on transient test methods for complicated heat transfer surfaces. Since then, transient testing methods have seen progress due to a number of investigators.

Rodriguez and Mills [8] adapted the single-blow transient testing technique, with a step-change in the inlet stream temperature, to analyze perforated plate heat exchangers and similar discontinuous surfaces. They formulated a set of coupled first order differential equations for the plate and fluid temperatures by applying energy balances to each of the plates in the exchanger. These equations were then solved numerically for a set of perforated plate heat exchangers containing a range of plate numbers, number of transfer units, and axial conduction parameters. Dimensionless maximum slopes were then presented in tabular form, allowing the heat transfer coefficient to be calculated from test data.

Liang and Yang [9] conducted a modified single-blow experiment to determine the convective heat transfer coefficients of surfaces. Accounting for the finite heat capacity of the heating screens used to implement the "step-change" in the inlet stream temperature, they modeled the fluid temperature jump as an exponential function. They then obtained an analytical solution using Laplace transforms and determined the heat transfer coefficient through a curve-matching technique. Their analysis unfortunately did not include axial conduction.

Stang and Bush [10] investigated heat transfer performance in a heat exchanger core by applying a periodic method. Realizing the experimental difficulty inherent in producing a step-change in the inlet fluid stream temperature, they implemented a more experimentally convenient periodic inlet stream temperature fluctuation and measured the temperature response of the outlet flow stream. They developed a mathematical model corresponding to such an inlet stream temperature condition, obtained test results for the periodic method, and conducted a critical comparison of the

[1]Corresponding author.

Contributed by the Heat Transfer Division of ASME for publication in the Journal of Heat Transfer. Manuscript received December 10, 2010; final manuscript received September 4, 2011; published online February 15, 2012. Assoc. Editor: Andrey Kuznetsov.

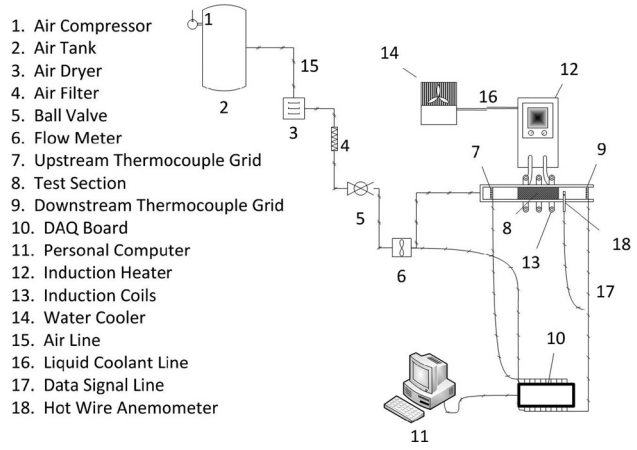

Fig. 1 Experimental configuration schematic

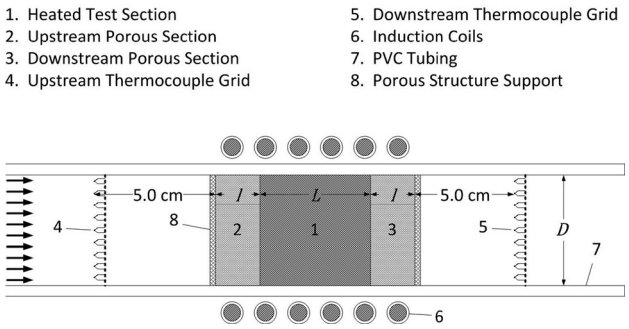

Fig. 2 Test section diagram, not shown to scale. Item # 8 in Fig. 1.

periodic method with the conventional single-blow method in which a step-change in the inflow stream temperature occurs. They concluded their study by listing the advantages of the periodic method over the step-change method.

Younis and Viskanta [11] experimentally investigated heat transfer by forced convection of air through porous ceramic foams using a single-blow transient technique. Employing a two-temperature model and implementing a step-change in the inlet air stream temperature, they obtained heat transfer coefficient correlations for a variety of foam specifications.

Recently, Nie et al. [12] determined the convective heat transfer coefficient for flow through particle beds using a new technique. Applying a step-change to the inlet air stream temperature, the transient experimental temperature distribution in the bed and the temperature at the outlet were obtained for the time interval during which the bed temperature distribution was essentially linear. These data were compared to a model in which the transient energy balance equations were integrated over the bed length and the specific time period in order to determine a correlation for the effective heat transfer coefficient in the bed.

Many of the transient tests used in the past to determine the heat transfer coefficients of complicated surfaces suffer from complications involving the experimental implementation of the inlet fluid stream temperature perturbation. Moreover, in general, numerous theoretical models exist for the different types of heat exchangers tested and it appears that none have clearly distinguished themselves from the others. It is the authors' intention in this paper to present a new technique, initially developed by Jones and Catton [13], to determine heat transfer characteristics of complex surfaces, i.e., compact heat exchangers, and to alleviate many of the inherent experimental inconveniences and modeling insufficiencies associated with other transient methods developed hitherto. To achieve this, we present an experimental method that utilizes a step-change in the solid phase heat generation rate via induction heating and a theoretical model based on VAT that may be applied to any porous structure provided that the morphology (i.e., the porosity and specific surface area) can be specified or assumed. This new transient method is then applied to determine the internal heat transfer coefficient in the core of a randomly packed bed of uniform spherical particles for which a number of correlations already exist. The study of the thermal characteristics of packed particle beds has merit due to their use in heat and mass exchangers, and for thermal energy storage applications.

Experimental Configuration

Upper scale steady state, fully-developed, one-dimensional flow conditions are achieved in a randomly packed bed of uniform steel spheres. The solid phase (steel) is subjected to a step-change in heat generation rate per unit volume from an induction heater. The transient gas phase exit temperature response is measured until steady state thermal conditions are achieved. A schematic of the experimental configuration is illustrated in Fig. 1.

The solid phase is a low carbon steel and the fluid is air. The tube in which the packed bed is contained is a polyvinyl chloride (PVC), providing a nearly adiabatic wall condition. The physical properties of the materials are tabulated in Table 1. A packed bed of identically sized polypropylene spheres is in contact with, and immediately upstream and downstream of, the heated test section, as illustrated in Fig. 2. The two packed bed segments of plastic spheres are of length l, where it was ensured that $l > 10d$ and $l > D$, and serve to eliminate fluid flow inlet and outlet effects, allowing a hydrodynamically fully-developed flow to enter the heated test section. Additionally, the two packed bed segments of plastic spheres ensure a uniform axial porosity in the heated section.

Three different test sections were examined. Their geometrical characteristics are tabulated in Table 2.

Two thermocouple grids are positioned upstream and downstream of the porous medium to measure the transient gas phase temperature response. A rotameter measures the gas flow rate, and an air velocity transducer measures the gas velocity distribution at the outlet (under nonheating conditions).

Table 1 Physical properties of the materials

		Solid phase (steel, at 100 °C)	Fluid phase (air, at 60 °C)	Wall (PVC, at 20 °C)
Mechanical	ρ (kg m^{-3})	7.87×10^3	1.070	1.4×10^3
	μ (kg m^{-1} s^{-1})		1.99×10^{-5}	
Thermal	k (W m^{-1} K^{-1})	6.03×10^1	2.79×10^{-2}	1.7×10^{-1}
	c_p (J kg^{-1} K^{-1})	4.82×10^2	1.006×10^3	1.05×10^3
Electrical	ρ_R (Ω m)	1.78×10^{-7}		
and magnetic[a]	μ_r (−)[b]	5×10^1		

[a]The Curie temperature, T_C, of the steel is 770 °C.
[b]Approximate representative value.

Table 2 Geometrical characteristics of the test sections

Test section	$d \times 10^3$ (m)	$D \times 10^2$ (m)	$L \times 10^2$ (m)	$l \times 10^2$ (m)
1	1.59	6.731	1.778	6.858
2	3.18	6.731	3.226	7.163
3	4.76	6.731	4.826	6.985

Heat Source

The solid phase is heated via induction heating. The induction heater used for the experiments described in this paper operated at a frequency on the order of 10^2 kHz (which is conventionally classified as a high frequency induction heat source) over the range of the experiments conducted and generated an output power on the order of 10^2 W. The induction coil used was of the basic solenoidal type and its geometric parameters, for each test section, are indicated in Table 3, where d_C and P_C are the diameter and pitch of the induction coil, and D_C is the solenoid diameter.

Rhee [14] examined the internal heat generation distribution in a randomly packed bed of stainless steel spherical particles subjected to a high frequency induction heat source. The particle bed was centered in a solenoidal work coil whose diameter, D_C, was approximately twice the diameter of the bed D. The particle bed Rhee examined was dimensionally similar to those considered in the present study (i.e., $d = 6.35$ mm, $D = 104$ mm, and $L = 26$ or 52 mm). Twenty thermocouples encased in thin glass tubes were distributed at various radial and axial locations in the bed. The heat generation was determined from the transient temperature response during heating. It was found that the difference between the mean value of the heat generation measurements and a single local value is less than 5%, indicating that the heat generation in the packed bed is essentially volumetrically uniform.

Somerton [15] conducted a similar experiment in which he used high frequency induction heating to heat a packed particle bed. The primary difference between Somerton's and Rhee's experiments is that Somerton's solenoidal copper work coil was tightly wrapped around the particle bed (i.e., $D_C \approx D$). Somerton presented plots of the radial and axial heat generation distribution for a typical case. It was found that the heat generation varied by about 7% in the radial direction. In the axial direction it was observed that the heat generation "profile is very flat with a slight tapering off of the power at the ends." Additionally, Cherng [16] conducted similar experiments on the uniformity of induction heating in a packed bed and came to a similar conclusion that the heat generation is essentially volumetrically uniform.

The lumped thermal capacity model is valid for each individual sphere provided that the sphere's internal resistance to heat transfer (i.e., conduction) is small compared to its external resistance (i.e., convection). The Biot number, Bi, characterizes the relative influence of internal and external resistances to heat transfer. For a sphere, $\mathrm{Bi} < 0.1$ is a suitable criterion for assuming that the particle has a spatially uniform temperature [17,18]. For the experiments considered here, the largest Biot number encountered Bi_{max}, neglecting conduction between particles, may be calculated, from Test Section 3 at $\mathrm{Re} = 500$ (see Results section), as

Table 3 Induction coil parameters. Copper coil, $d_c = 9.5$ mm, and $P_C = 1.27$ cm. The coils are internally cooled with deionized water, flowing in a closed loop, from a water cooler.

Test section	No. of coil turns	D_C (cm)
1	2	16.51
2	3	16.51
3	4	13.97

$$\mathrm{Bi}_{max} = \frac{h(d/6)}{k_s} = \frac{(307\ \mathrm{Wm^{-2}K^{-1}})(4.76 \times 10^{-3}\ \mathrm{m})}{6(65.2\ \mathrm{Wm^{-1}K^{-1}})} = 3.7 \times 10^{-3} < 0.1 \quad (1)$$

where the characteristic length is the ratio of the particle's volume to its surface area. The lumped thermal capacity model is therefore applicable to each spherical particle in the bed for these experiments, indicating that a uniform temperature profile exists in each particle as it undergoes its transient thermal response.

Distinguishing the Near-Wall and Core Regions. It is known that there exists a radial variation in void fraction within a randomly packed bed of uniform spheres. In particular, Benenati and Brosilow [19] demonstrated that void fraction is unity at the wall and follows a damped oscillatory function to an essentially constant value of 0.39 in the core of the bed, about four to five sphere diameters in from the wall. This void fraction profile is due to the point contact between the spheres and the container wall, the highly ordered structure they attain near the wall, and the gradual influence of the random packing as the bed's core is approached from the wall. Martin [20] presented the following expression for the porosity profile $\varepsilon(z)$

$$\varepsilon(z) = \begin{cases} \varepsilon_{min} + (1 - \varepsilon_{min})z^2, & -1 \le z \le 0 \\ \varepsilon_c + (\varepsilon_{min} - \varepsilon_c)\exp(-z/4)\cos\left(\pi\sqrt{3/2}z\right), & z \ge 0 \end{cases} \quad (2)$$

where $z = 2(y/d) - 1$ and y is the radial distance from the wall. Investigators such as Achenbach [21] and Ziółkowska and Ziółkowski [22] have noted that this voidage profile leads to a bypass or channeling effect, that is, preferential flow near the wall of the packed bed, since pressure drop is strongly dependent upon porosity, and in particular, when the bed is heated, leads to a cold flow bypass in the near-wall region. The effect of a cold flow bypass in our experiment, if not accounted for, is to decrease the measured value of the heat transfer coefficient. Some researchers, such as Kays and London [2], specify that they are looking at an "infinite" packed bed, in which the wall effects are negligible. Ziółkowska and Ziółkowski [22] give a criterion for determining the ratio of tube to particle diameter, D/d, at which wall effects are negligible, namely, $D/d \ge 120$. Such a criterion is not realized for some test rigs and for some experimental methods. Moreover, many examples of packed beds used in industrial processes do not meet this requirement, preventing them from being modeled by a uniform radial porosity.

Measurements of the velocity profile in a randomly packed bed of uniform spherical particles were obtained and are presented, along with the porosity profile, in Fig. 3. Schlünder [23] proposed

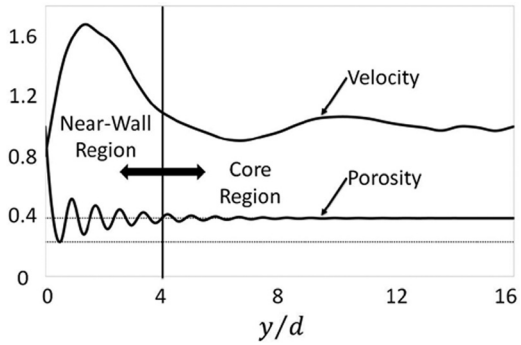

Fig. 3 Near-wall porosity and preferential flow (velocity is scaled with centerline velocity) in a randomly packed bed of uniform spheres (spheres were not heated), Test Section 1, Re = 305. Porosity distribution taken from the formula given in Eq. (2), where $\varepsilon_C = 0.39$, and $\varepsilon_{min} = 0.23$.

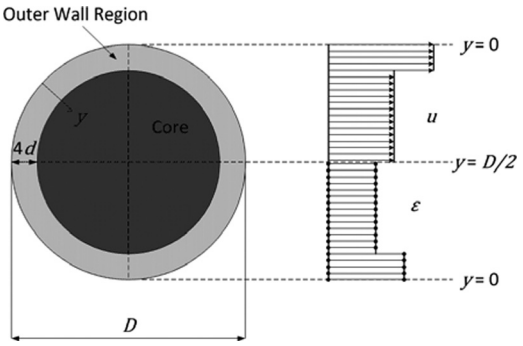

Fig. 4 Modeling the near-wall bypass or channeling effect

that for a packed bed, which is finite in the radial direction, one may divide the area perpendicular to the flow direction into a near-wall region and a core region. One then assumes uniform voidage and flow in each section. Schlünder's success, and that of others ([24], for example), with this method has led us to consider analyzing the core of our packed bed as separate from the near-wall region. Schlünder defined the near-wall region to be within a distance of $0.5d$ from the wall, because the average porosity remains practically constant at 0.39 beyond this point, and is equal to 0.50 within. From Fig. 3 it is apparent that one may define a so called "near-wall region" within four sphere diameters from the wall, and a "core region" beyond the near-wall region. Unlike Schlünder's definition which is based on porosity distribution considerations, the near-wall region definition used in this study is based on measured velocity profiles for the cases under consideration, a more applicable definition for this study in the authors' opinion. This definition of the near-wall and core regions will be taken in our analysis and is illustrated in Fig. 4.

Measurements of the velocity profile in our three test sections were made at several flow rates for each test section. A calibrated air velocity transducer was used and 10^3 measurements were made for each test section and each flow rate at various radial and circumferential locations 1.50 cm above the packed bed outlet. The Dupuit-Forchheimer hypothesis [25] relates the interstitial velocity u to the superficial or apparent velocity U, measured by the air velocity transducer, and the bed porosity, $u = U/\varepsilon$. From these measurements we can determine the dependence of core velocity on the overall measured flow rate for each test section. Figure 5 plots the ratio of core superficial velocity U to upstream superficial velocity U' for our three test sections over the flow rate ranges

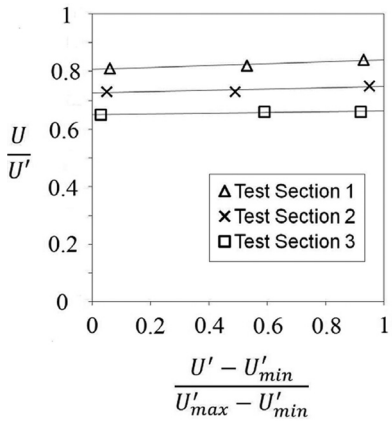

Fig. 5 Measured ratio of core superficial velocity U to upstream superficial velocity U' for the three test sections over the flow rate ranges in each. U'_{min} and U'_{max}, respectively correspond to the minimum and maximum flow rates achieved in the experiment for each of the three test sections.

Table 4 Core to upstream superficial velocity ratios, ±7%

	Test section 1	Test section 2	Test section 3
U/U'	0.83	0.74	0.66

considered for each test section. The upstream superficial velocity is related to the overall flow rate through the test section $\dot{m}'$, measured by the rotameter, by

$$U' = \frac{\dot{m}'}{\rho A'} \tag{3}$$

where A' is the cross-sectional area of the test section. The core superficial velocity may be expressed, similarly, as

$$U = \frac{\dot{m}}{\rho A} = \frac{\dot{m}''}{\rho} \tag{4}$$

where $\dot{m}$ is the mass flow rate through the core of the test section, $\dot{m}''$ is the mass flux through the core of the test section, and A is the cross-sectional area of the core of the test section. The ratio of core to superficial velocities may be expressed as

$$\frac{U}{U'} = \frac{\dot{m}''}{(\dot{m}'/A')} \tag{5}$$

where $(\dot{m}'/A')$ is the overall mass flux through the test section. It is apparent from our measurements that while the bypass effect is highly dependent upon the ratio of particle to tube diameter, it depends little upon the flow rate. In Table 4, the core to upstream superficial velocity ratio used to correct the rotameter readings for each flow rate is stated for each test section along with the uncertainty in its value.

Just as the velocity is taken at the core of the packed bed for our analysis, the fluid temperature response is also taken at the outlet of the core of the packed bed. The thermocouple grid at the outlet allows several transient fluid temperature response measurements to be made across the packed bed core for each experimental run. The average of these core flow temperature measurements are input into the solution algorithm. The spread in their values is used in assessing uncertainty in the solution.

Although turbulent flow within a packed bed on the lower scale is three-dimensional and chaotic, dividing the packed bed into a near-wall and a core region has precedent as a successful strategy (as demonstrated in Refs. [23,24]), and thus we have decided to adopt it.

Model Assumptions

Travkin and Catton [26] rigorously derived the VAT-based equations governing fluid flow and heat transfer in porous media. Due to the averaging process, the VAT-based governing equations yield additional integral and differential terms when compared to the homogenized or classical continuum mechanics equations. Travkin and Catton devoted some effort to relate these additional terms to the transport coefficients—h and the friction factor, f—and the morphology functions—ε and S. With these four terms known the governing equation set is closed and readily solvable.

In this work, a two-temperature macroscopic volume averaging technique is used to develop the basic relations [27]. The model is one-dimensional and it is assumed that heat is only generated within the solid phase. Forced convection is assumed to be the main convective process, and convective energy transport between the phases manifests itself as sources within each energy equation. Fluid phase conduction is assumed negligible, and solid phase conduction in the radial direction and radiation transport in the radial direction are not considered in this analysis.

Thermally (and hydrodynamically) incompressible flow is assumed. By keeping the experimental temperatures relatively low this assumption will hold and we can avoid the additional complexity of solving the mass and momentum equations, thereby reducing the modeling requirements to just the gas and solid phase thermal energy equations.

Although the transient spatial temperature profiles of the solid and fluid cannot be directly obtained experimentally, they can be inferred from the numerical simulation. Transient and spatial temperature variations could affect solid and fluid properties, the effective thermal conductivity, and the solid phase heat generation rate. However, maintaining relatively low experimental temperatures allows us to make an Oberbeck–Boussinesq approximation and assume constant properties, a constant effective thermal conductivity, and a constant heat generation rate, greatly simplifying the analysis.

In developing the governing equations, several assumptions are made about the geometrical properties of the porous medium. An appropriately modeled geometry is necessary to perform the VAT based numerical simulations. The volumetric porosity, ε, of the medium is assumed constant throughout, and for the core section of a randomly packed bed of spheres is taken to be 0.39. This value for the porosity is commonly cited in the literature, see for example [19].

The specific surface area, S, defined as the interfacial surface area per unit volume, is considered next. For the simple case of a packed bed of spheres, the specific surface area can be determined easily from geometrical considerations to be

$$S = \frac{6(1-\varepsilon)}{d} \tag{6}$$

Fluid Phase Temperature

For one-dimensional flow through a porous medium the change in fluid energy stored within a control volume can be written as the sum of the flux of energy into the control volume and the convective transport from the solid phase. This can be expressed in differential form as

$$\rho_f c_{p_f} \varepsilon \frac{\partial T_f}{\partial t} + \rho_f c_{p_f} \varepsilon u \frac{\partial T_f}{\partial x} = hS(T_s - T_f) \tag{7}$$

It will be convenient to write the solid and fluid phase dimensionless temperatures in terms of a characteristic temperature difference ΔT_f (defined later in Eq. (22)) as

$$\theta_f = \frac{T_f - T_{in}}{\Delta T_f}, \quad \theta_s = \frac{T_s - T_{in}}{\Delta T_f} \tag{8}$$

respectively, where T_{in} is the inlet gas phase temperature, and initial temperature of the solid and fluid. The dimensionless velocity can be defined in terms of the mean interstitial velocity, u_0, or the upstream superficial velocity U, as

$$\hat{u} = \frac{u}{u_0} = \frac{u\varepsilon}{U} \tag{9}$$

It is also convenient to scale the spatial coordinate by the porous medium length, L, and the temporal coordinate by a characteristic time, τ, as

$$\hat{x} = \frac{x}{L}, \quad \hat{t} = \frac{t}{\tau} \tag{10}$$

respectively. The characteristic time, τ, is defined as

$$\tau = \frac{L}{u_0} = \frac{\varepsilon L}{U} \tag{11}$$

which may be viewed as the average time it takes for a fluid particle to traverse the porous medium's length.

With the above definitions we can write the fluid phase temperature differential equation in dimensionless form as

$$\frac{\partial \theta_f}{\partial \hat{t}} + \hat{u}\frac{\partial \theta_f}{\partial \hat{x}} = \frac{hSL}{\rho_f c_{p_f} U}(\theta_s - \theta_f) \tag{12}$$

Assuming the fluid to be incompressible, $u = U/\varepsilon = u_0$ and thus $\hat{u} = 1$. Therefore, the mass and momentum equations can be discarded.

We can now write the dimensionless gas phase temperature differential equation as

$$\frac{\partial \theta_f}{\partial \hat{t}} + \frac{\partial \theta_f}{\partial \hat{x}} = \frac{hSL}{\rho_f c_{p_f} U}(\theta_s - \theta_f) \tag{13}$$

Solid Phase Temperature

For one-dimensional thermal considerations in a porous medium, the change in solid phase energy stored within a control volume can be written as the sum of energy conduction (effective) into the control volume, energy transport from the fluid phase, and internal heat generation (solid phase only). This can be expressed in differential form as

$$\rho_s c_{p_s}(1-\varepsilon)\frac{\partial T_s}{\partial t} = k_{eff}\frac{\partial^2 T_s}{\partial x^2} + hS(T_f - T_s) + \dot{Q}'''(1-\varepsilon) \tag{14}$$

Here, it is worth noting that the effective thermal conductivity has been defined over the entire cross-sectional area of the medium, rather than over the area of the solid phase. This convention is simply for convenience.

Nondimensionalizing the above solid phase temperature differential equation, we obtain

$$\frac{\partial \theta_s}{\partial \hat{t}} = \frac{\varepsilon}{(1-\varepsilon)}\frac{k_{eff}}{\rho_s c_{p_s} LU}\frac{\partial^2 \theta_s}{\partial \hat{x}^2} + \frac{\varepsilon}{(1-\varepsilon)}\frac{hSL}{\rho_s c_{p_s} U}(\theta_f - \theta_s) + \frac{\dot{Q}'''L\varepsilon}{\rho_s c_{p_s}\Delta T_f U} \tag{15}$$

Dimensionless Numbers

Several dimensionless numbers are of interest. The Nusselt, Reynolds, and Prandtl numbers are defined, respectively, as

$$\mathrm{Nu} = \frac{hd_h}{k_f} = \frac{4h\varepsilon}{Sk_f} \tag{16}$$

$$\mathrm{Re} = \frac{\rho_f u_0 d_h}{\mu_f} = \frac{4\rho_f u_0 \varepsilon}{\mu_f S} = \frac{4\rho_f U}{\mu_f S} \tag{17}$$

$$\mathrm{Pr} = \frac{c_{p_f}\mu_f}{k_f} = \frac{\nu_f}{\alpha_f} \tag{18}$$

It should be noted that the hydraulic diameter d_h is defined as

$$d_h = \frac{4\varepsilon}{S} \tag{19}$$

This definition follows from the classic definition of hydraulic diameter for internal flows.

Another dimensionless parameter which arises is the hydraulic diameter to length ratio, χ, defined as

$$\chi = \frac{d_h}{L} = \frac{4\varepsilon}{SL} \tag{20}$$

Characteristic Temperature Difference

At steady state, all energy generated by inductive heating is transferred to the gas phase, assuming minimal lateral losses (due

to radiation or natural convection, for example). Therefore, the characteristic temperature difference used to scale both the solid and fluid temperatures can be defined as the fluid temperature response across the porous medium at steady state. Performing an energy balance on the porous medium gives

$$\dot{Q}''' V_s = \dot{m}''_f c_{p_f} A_{s+f} \Delta T_f \tag{21}$$

Here, we have defined the mass flux in terms of the solid and fluid cross-sectional areas (as we did for the effective thermal conductivity). Solving the energy balance for the characteristic temperature difference ΔT_f gives

$$\Delta T_f = \frac{\dot{Q}''' V_s}{\dot{m}''_f c_{p_f} A_{s+f}} = \frac{\dot{Q}''' L(1-\varepsilon)}{\dot{m}''_f c_{p_f}} \tag{22}$$

where geometrical considerations have been employed.

This relation for ΔT_f can be substituted into the solid phase temperature differential equation, Eq. (15), to yield

$$\frac{\partial \theta_s}{\partial \hat{t}} = \frac{\varepsilon}{(1-\varepsilon)} \frac{k_{eff}}{\rho_s c_{p_s} LU} \frac{\partial^2 \theta_s}{\partial \hat{x}^2} + \frac{\varepsilon}{(1-\varepsilon)} \frac{hSL}{\rho_s c_{p_s} U} (\theta_f - \theta_s) + \frac{\varepsilon}{(1-\varepsilon)} \frac{\rho_f c_{p_f}}{\rho_s c_{p_s}} \tag{23}$$

Governing Equations

The fluid and solid phase temperature differential equations can now be expressed in terms of the dimensionless numbers. The fluid and solid phase temperature differential equations are

$$\frac{\partial \theta_f}{\partial \hat{t}} + \frac{\partial \theta_f}{\partial \hat{x}} = \frac{4\mathrm{Nu}}{\chi \mathrm{Re}\,\mathrm{Pr}} (\theta_s - \theta_f) \tag{24}$$

$$\frac{\partial \theta_s}{\partial \hat{t}} = \frac{1}{(1-\varepsilon)} \frac{(\alpha_s/\alpha_f)}{(k_s/k_{eff})} \frac{\chi}{\mathrm{Re}\,\mathrm{Pr}} \frac{\partial^2 \theta_s}{\partial \hat{x}^2} + \frac{4\varepsilon}{(1-\varepsilon)} \frac{\rho_f c_{p_f}}{\rho_s c_{p_s}} \frac{\mathrm{Nu}}{\chi \mathrm{Re}\,\mathrm{Pr}} (\theta_f - \theta_s) + \frac{\varepsilon}{(1-\varepsilon)} \frac{\rho_f c_{p_f}}{\rho_s c_{p_s}}. \tag{25}$$

Inspection of these two relations suggests that the problem can be characterized in terms of three dimensionless parameters

$$\alpha = \frac{4\mathrm{Nu}}{\chi \mathrm{Re}\,\mathrm{Pr}} \tag{26}$$

$$\beta = \frac{\varepsilon}{1-\varepsilon} \frac{\rho_f c_{p_f}}{\rho_s c_{p_s}} \tag{27}$$

$$\gamma = \frac{k_{eff}}{k_f} \frac{\chi}{\varepsilon \mathrm{Re}\,\mathrm{Pr}} \tag{28}$$

Inspection of these parameters reveals that they are essentially the Stanton number, the heat capacity ratio, and a thermal conductivity parameter, respectively. Substitution of these parameters into the fluid and solid phase temperature differential equations reduces the governing equations to the following rather simple forms

$$\frac{\partial \theta_f}{\partial \hat{t}} + \frac{\partial \theta_f}{\partial \hat{x}} = \alpha(\theta_s - \theta_f) \tag{29}$$

$$\frac{\partial \theta_s}{\partial \hat{t}} = \alpha\beta(\theta_f - \theta_s) + \beta + \beta\gamma \frac{\partial^2 \theta_s}{\partial \hat{x}^2} \tag{30}$$

Initial Conditions

Since both the solid and fluid temperatures, $\theta_s(\hat{x}, \hat{t})$ and $\theta_f(\hat{x}, \hat{t})$, have been scaled with respect to the fluid inlet temperature and the system begins with no heating, the initial conditions are

$$\theta_s(\hat{x}, 0) = \theta_f(\hat{x}, 0) = 0 \tag{31}$$

Boundary Conditions

The boundary conditions used for the numerical solution are given by the inlet gas temperature and two solid phase adiabatic conditions

$$\theta_f(0, \hat{t}) = \left.\frac{\partial \theta_s(\hat{x}, \hat{t})}{\partial \hat{x}}\right|_{\hat{x}=0} = \left.\frac{\partial \theta_s(\hat{x}, \hat{t})}{\partial \hat{x}}\right|_{\hat{x}=1} = 0 \tag{32}$$

Numerical Methods and Solution Algorithm

With knowledge of the fluid and solid material properties, fluid flow rate, geometrical configuration, and the heat transfer characteristics we can perform a numerical simulation by solving the above governing equations. A fully explicit numerical scheme is employed and all of the spatial derivatives are centrally differenced. The spatial discretization splits the porous medium into Eq. (40) equally spaced nodes spanning the streamwise dimension of the porous medium sample. Solutions are obtained at integral values of the dimensionless time ($\hat{t} = t/\tau$), which depends on the flow conditions. The simulation yields the solid and fluid phase temperatures as a function of time and space.

The governing equation parameters must be known to perform the simulation, however, α and γ contain the heat transfer coefficient, h, and the effective thermal conductivity, k_{eff}, respectively, both of which are unknown at this point. It is shown below (in section Effective Thermal Conductivity) that the determination of the internal heat transfer coefficient is independent of the value of the effective thermal conductivity, and that 20 W m^{-1} K^{-1} is an appropriate value for the simulation. The heat transfer coefficient, h, is then the only unknown remaining. If we knew the correct value for h we could perform the simulation. We can use this fact along with the experimental data to find the correct value of the heat transfer coefficient, expressed in terms of the Nusselt number. In other words, we can "back out" h from the experimental data by matching the simulated response profile corresponding to that h with the experimental response profile.

Simulated Fluid Temperature Response. The simulated dimensionless fluid temperature response is given the symbol δ_{sim} and is a function of the dimensionless time $\hat{t}$. It is defined as

$$\delta_{sim}(\hat{t}) = \theta_f(1, \hat{t}) - \theta_f(0, \hat{t}) \tag{33}$$

That is, the simulated dimensionless fluid temperature response is the difference between the dimensionless fluid temperature values at the outlet and inlet of the test section. Recalling the definition of the dimensionless fluid temperature θ_f, δ_{sim} may be rewritten as

$$\delta_{sim} = \frac{T_f(1, \hat{t}) - T_f(0, \hat{t})}{\Delta T_f} = \frac{T_{out} - T_{in}}{\Delta T_f} \tag{34}$$

where T_{in} and T_{out} are the simulated dimensional fluid inlet and outlet temperatures, respectively. The code extracts the simulated dimensionless transient fluid temperature response profile from the full simulation. δ_{sim} is determined at integral dimensionless time values up to the point at which steady state thermal conditions are achieved. The time it takes for our system to reach steady state thermal conditions is determined from experimentally considering the outlet fluid temperature. A typical graph of the simulated response δ_{sim} versus time $\hat{t}$ is given in Fig. 6.

Experimental Fluid Temperature Response. The experimental dimensionless fluid temperature response is given the symbol δ_{exp}. To obtain δ_{exp} as a function of dimensionless time, the raw experimental temperature versus time data is gathered. The raw inlet and outlet temperature data are known in degrees Celsius, at

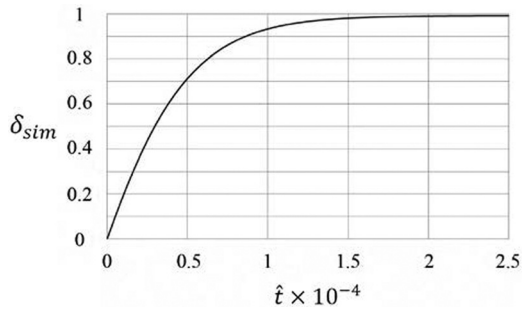

Fig. 6 Simulated dimensionless transient fluid temperature response profile

raw time values given in seconds. The data are scanned to determine the minimum and maximum experimental dimensional temperature values, denoted by $T^*_{\min}$ and $T^*_{\max}$, respectively, where the superscript explicitly denotes experimental values. The experimental dimensional outlet temperature, denoted by T^*_{out}, is known at discreet dimensional times. $T^*_{\min}$, $T^*_{\max}$, and T^*_{out} are used to define $\delta_{\exp}$. It is desired to know T^*_{out} at integral values of the dimensionless time in order to compare $\delta_{\exp}(\hat{t})$ with $\delta_{\text{sim}}(\hat{t})$. That is, we wish to know T^*_{out} at $t = 0,\tau,2\tau,3\tau,\ldots,N\tau$, where $N\tau$ is the raw time at which steady state thermal conditions have been achieved. To obtain T^*_{out} at integral values of the dimensionless time up to steady state, the experimental data set is first reduced by only considering the data that occur from the time of zero up to $t = N\tau$, and then $N+1$ points which span this duration evenly are interpolated to obtain $T^*_{\text{out}}(\hat{t})$ for $\hat{t} = 0,1,2,3,\ldots,N$. The experimental dimensionless fluid temperature response as a function of the dimensionless time is then defined as

$$\delta_{\exp}(\hat{t}) = \frac{T^*_{out}(\hat{t}) - T^*_{\min}}{\left(T^*_{\max} - T^*_{\min}\right)} \tag{35}$$

$T^*_{\min}$ can be seen as the experimental fluid inlet temperature (or initial temperature) and may be expressed as T^*_{in}. $(T^*_{\max} - T^*_{\min})$ can be seen as the temperature increase of the fluid at steady state, corresponding to an experimental characteristic temperature difference. This experimental characteristic temperature difference may be expressed as ΔT^*_{f}. With this new notation, $\delta_{\exp}$ may be written as

$$\delta_{\exp} = \frac{T^*_{\text{out}} - T^*_{\text{in}}}{\Delta T^*_{\text{f}}} \tag{36}$$

illustrating the comparability of $\delta_{\exp}$ and δ_{sim}, see Eq. (34). A typical graph of the experimental response $\delta_{\exp}$ versus time $\hat{t}$ is given in Fig. 7.

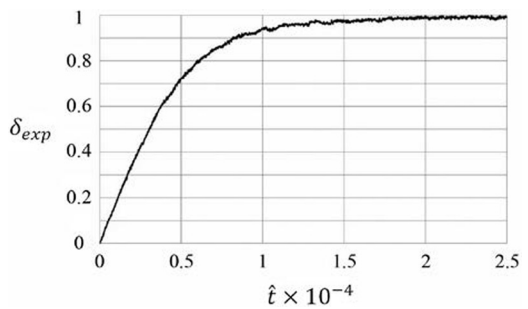

Fig. 7 Experimental dimensionless transient fluid temperature response profile

Steady State Definition. In considering the experimental dimensionless transient fluid temperature response profile and characterizing $(T^*_{\max} - T^*_{\min})$ as the "experimental characteristic temperature difference" ΔT^*_{f}, we have made a statement about when steady state thermal conditions are achieved. $T^*_{\max}$ can be expected to occur at, or very close to $\hat{t} = N$. Therefore, in our analysis, steady state occurs at $\hat{t} = N$. In selecting an appropriate value for N, we must examine experimental data and decide when steady state experimental conditions are achieved. It was determined that a value of $N = 25{,}000$ is an appropriate value for our test section and Reynolds number range, see Figs. 6 and 7. It is found that this value of N allows the code to adequately balance the importance of matching both the initial steep change in fluid temperature response with time and the more gradual change in fluid temperature response with time leading up to steady state conditions. If N is much higher the code puts unnecessary importance on matching steady state conditions, which is a trivial concern. If N is much lower the code fails to consider matching much of the highly transient portion of the fluid temperature response versus time profile.

Iteration and Convergence. In determining the error between the simulated and experimental dimensionless transient fluid temperature response profiles a mean squared error E is used, and is defined as

$$E = \sqrt{\sum_{\hat{t}=0}^{25{,}000} \left[\delta_{\exp}(\hat{t}) - \delta_{\text{sim}}(\hat{t})\right]^2} \tag{37}$$

During the iteration procedure the simulated fluid temperature response profile varies with the Nusselt number. The objective of the iteration is to hone in on the value of the Nusselt number that yields a close match between the simulated and experimental temperature response profiles. That is, the objective of the iteration is to minimize E. A typical iteration sequence is illustrated in Fig. 8.

Effective Thermal Conductivity

It has been found in this study that the value of the effective thermal conductivity has negligible influence on the determination of the internal heat transfer coefficient. This can be observed in Fig. 9, where the value of the effective thermal conductivity is varied over a wide range, yet the transient fluid temperature response profile is hardly affected by this variation. Travkin and Catton [26] show this using fundamental arguments. Figure 9 can be compared to Fig. 10, where the value of h is varied over a considerably smaller range yet the temperature profiles are clearly distinguishable provided that h is not too high. For a high enough h the two-temperature model will break down, and this experimental method is not viable unless the surface area of the porous structure is decreased by decreasing L, or the product, $\dot{m}c_{\text{p}}$, is increased by changing the working fluid. Additionally, a scaling analysis shows that in the solid phase energy equation, Eq. (30),

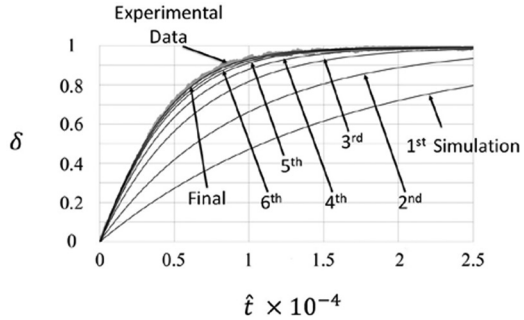

Fig. 8 Iteration sequence

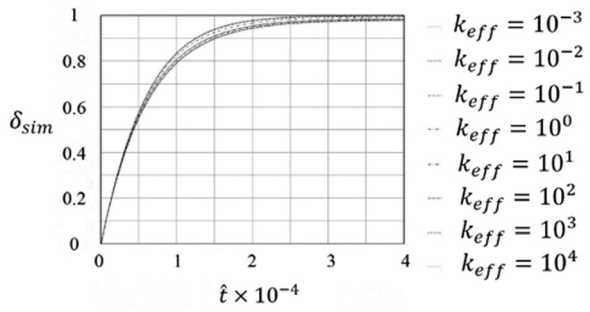

Fig. 9 Variation of δ_{sim} versus $\hat{t}$ with effective thermal conductivity (W m^{-1} K^{-1}). Nusselt number is unity, Re = 300.

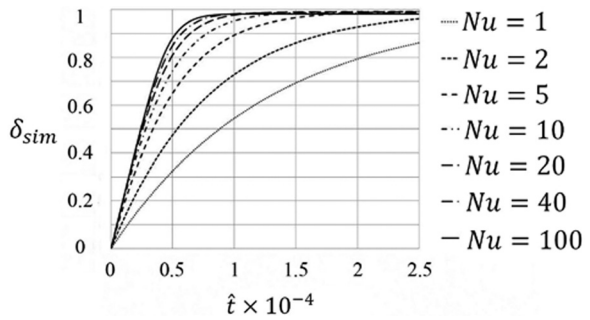

Fig. 10 Variation of δ_{sim} Versus $\hat{t}$ with Nusselt number. k_{eff} = 20Wm^{-1}K^{-1}, Re = 300

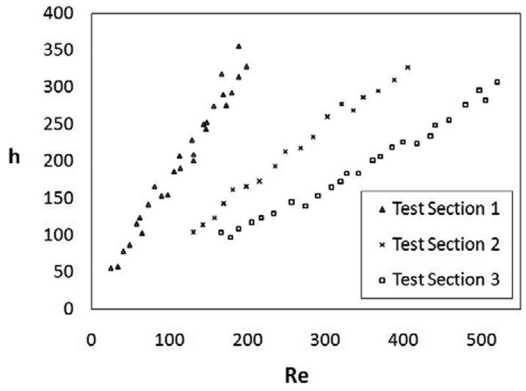

Fig. 11 Experimental heat transfer coefficient data

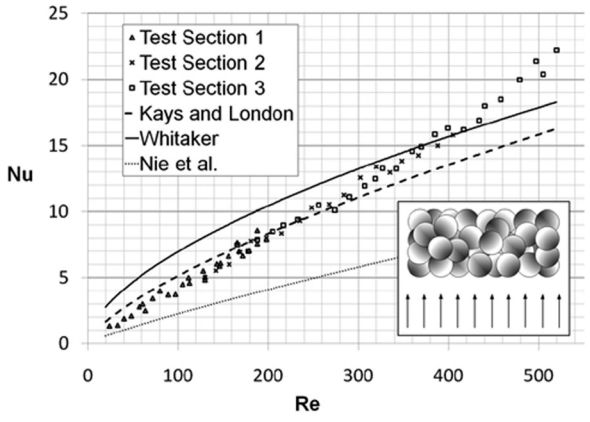

Fig. 12 Experimental data for Test Sections 1, 2, and 3. Correlations are from Kays and London [2], Whitaker [29], and Nie et al. [12].

the conduction term is two orders of magnitude less than the transport and generation terms, for our experiments, and thus plays a small role in the solution.

With this understanding we may adopt an approximate value for the effective thermal conductivity as 20 W m^{-1} K^{-1} by referring to Wakao and Kato [28] for our values of k_s and k_f, knowing that the particular value of k_{eff} has negligible influence on the determination of h.

Results

The experimental heat transfer coefficient results for Test Sections 1, 2, and 3 are plotted in Fig. 11. In Figure 12, the Nusselt number data are presented along with the well known correlations for packed beds of spheres of Kays and London [2] and Whitaker [29], and the very recent correlation of Nie et al. [12], all of which have been expressed in terms of the parameters defined in Eqs. (16) through (18). From our experimental data, we obtain the following new correlation for the Nusselt number as a function of the Reynolds and Prandtl numbers

$$\mathrm{Nu} = 0.057\mathrm{Re}^{0.96}\,\mathrm{Pr}^{1/3} \tag{38}$$

This correlation is valid for Reynolds numbers between 20 and 500 and is expected to be valid at reasonable limits beyond this. Although the effect of varying Prandtl number was not investigated here, a one-third power law is precedent, for gas flows, from other studies [2,12,29]. For liquid flows, $\mathrm{Pr}^{1/3}$ may not be accurate. This correlation is superimposed on a graph of a multitude of porous media convective heat transfer correlations obtained from Travkin and Catton [26] in Fig. 13.

Uncertainty Analysis

The remaining error, E, in the iteration scheme, after convergence has been obtained, is small (<5). It is essentially due to noise in the thermocouple readings causing the experimental data to be slightly scattered about the converged simulation, see Fig. 8. Therefore, the remaining value of E after convergence is obtained should receive no further consideration.

The temperature measurements themselves are subject to uncertainty. Although the thermocouples were calibrated, and radiation

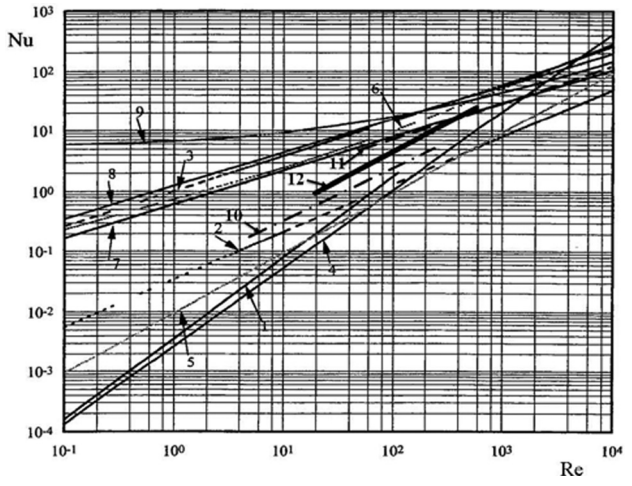

Fig. 13 Internal effective heat transfer coefficient in porous media, reduced based on VAT scale transformations, from experiments by 1, Kar and Dybbs [30] for laminar regime; 2, Rajkumar [31]; 3, Achenbach [21]; 4, Younis and Viskanta [11]; 5, Galitseysky and Moshaev [32]; 6, Kokorev et al. [33]; 7, Gortyshov et al. [34]; 8, Kays and London [2]; 9, Heat Exchangers Design Handbook [35]; 10, Nie et al. [12]; 11, Whitaker [29]; 12, Eq. (38). Adapted from Travkin and Catton [26].

losses (to the colder walls) and gains (from the hotter packed bed) are negligible (<2%), the core fluid phase temperature response is subject to uncertainty due to the random nature of the flow and heat transfer within the core of the packed bed at the lower scale. The various core temperature response measurements differ slightly from each other and so when taking the average core fluid phase temperature response some uncertainty is introduced. That is, there are some thermocouple recordings that yields slightly higher heat transfer coefficients than the bulk mixing cup average of the readings, and other thermocouple recordings that yield slightly lower heat transfer coefficients.

Perhaps the most significant measurement uncertainty is that associated with the core velocity due to the strong influence of flow rate on convective heat transfer. The rotameter and air velocity transducer are accurate themselves, yet when determining the ratio of core superficial velocity to upstream superficial velocity for our three test sections using the air velocity transducer, the flow being measured was highly turbulent. Measuring such a turbulent, spatially varying flow introduces significant uncertainty into our reduced flow rates.

The uncertainties in the temperature and flow rate measurements were propagated using the code, and uncertainties in Nusselt number were obtained for various Reynolds numbers. From this analysis, it is seen that the correlation, Eq. (38), is accurate to within 15% for the range of Reynolds numbers under consideration.

Discussion

From Fig. 12, it is apparent that the experimental results obtained in this study compare in magnitude reasonably with the established correlations for the internal heat transfer coefficient in packed beds of spheres. The exponent in the Reynolds number obtained here, however, is higher than that in the established correlations. Let us discuss these correlations and how they compare with the present results in more detail.

Whitaker's correlation [29], reduced based on the VAT scale definitions in Eqs. (16) through (18)

$$\mathrm{Nu} = \left[\frac{1}{3}\left(\frac{3}{2}\mathrm{Re}\right)^{1/2} + \frac{2}{15}\left(\frac{3}{2}\mathrm{Re}\right)^{2/3}\right]\mathrm{Pr}^{1/3} \tag{39}$$

was obtained from correlating a large amount of data for various packings from a wide range of researchers. It has been used successfully as an approximation but is not intended to be the most accurate correlation. Our correlation sees good agreement with Whitaker's, particularly at higher flow rates.

Kays and London's correlation [2]

$$\mathrm{Nu} = 0.23\mathrm{Re}^{0.7}\,\mathrm{Pr}^{1/3} \tag{40}$$

written based on the definitions used in this paper, was obtained by implementing a standard single-blow transient testing technique to an "infinite" packed bed of spheres, whereby a step-change in the inlet air temperature produced a transient outlet temperature profile whose maximum slope allowed h to be deduced from an analysis. The analysis used was based on the early Anzelius and Schumann analysis of heat transfer to an idealized porous body [4,36]. This correlation sees reasonable agreement with Eq. (38), particularly at lower flow rates.

The results obtained in this study lie above those recently obtained by Nie et al. [12] for a packed bed of spheres. Their correlation for the Nusselt number is written, based on the definitions in this paper, as

$$\mathrm{Nu} = 0.0491\mathrm{Re}^{0.8572}\,\mathrm{Pr}^{1/3} \tag{41}$$

Like the test sections examined in this study, they looked at packed beds for which near-wall preferential flow was present ($16 \leq D/d \leq 51$). Our correcting for the bypass effect played a role in Eq. (38) being higher than their correlation.

It can also be observed from Fig. 12 that the results are independent of the size of the spheres. This is evident in the considerable overlap of the results for each test section, seen over the Reynolds number range of about 100–400, and the application of a single correlation for all three test sections. This observation allows broad application of Eq. (38).

Conclusion

A new method for determining the internal heat transfer coefficient in porous media was developed and applied to a randomly packed bed of uniform spherical particles. Near-wall preferential flow in a packed bed was experimentally observed and accounted for in the analysis by adopting methods that have previously shown success. Experimental results for the Nusselt number over a Reynolds number range of 20–500 were obtained for the core of three different randomly packed beds of spheres, and a new correlation was presented. This correlation is seen to be in reasonably good agreement with the results of other investigators.

It was observed in our study that the internal heat transfer coefficient is essentially independent of the effective thermal conductivity. This observation allows the initial two parameter problem to be approached as a one parameter problem, greatly simplifying the task.

The presence of near-wall preferential flow in packed beds was noted. It is suspected that this phenomenon may contribute to the smaller measured Nusselt number values in finite packeds beds compared to those in "infinite" packed beds. A method was implemented to account for such near-wall preferential flow by looking solely at the core of the packed bed, as the core of a finite packed bed resembles an infinite packed bed in its structure.

Additionally, we observed the independence of the packed bed's sphere diameters in our results. This was also noticed recently by Nie et al. [12].

The technique developed in this paper shows promise as a convenient, state-of-the-art tool for exploring internal convective heat transfer coefficients associated with fluid flow through porous solid structures.

Acknowledgment

The support of the DARPA MACE program Grant No. W31P4Q-09-1-0005 is gratefully acknowledged. The views, opinions, and/or findings contained in this article are those of the authors and should not be interpreted as representing the official views or policies, either expressed or implied, of the Defense Advanced Research Projects Agency or the Department of Defense.

Nomenclature

A = core cross-sectional area, m^2
A' = test section cross-sectional area, m^2
Bi = Biot number
c_p = specific heat, $\mathrm{J\,kg^{-1}\,K^{-1}}$
d = sphere diameter, m
D = test section diameter, m
d_h = hydraulic diameter, m
f = frequency of the ac field of the work coil, $\mathrm{s^{-1}}$, friction factor
E = mean squared error
h = internal heat transfer coefficient, $\mathrm{W\,m^{-2}\,K^{-1}}$
k = thermal conductivity, $\mathrm{W\,m^{-1}\,K^{-1}}$
L = length of test section, m
l = length of upstream adiabatic flow development section, m
m = mass, kg
$\dot{m}$ = mass flow rate through the core of the test section, $\mathrm{kg\,s^{-1}}$
$\dot{m}'$ = overall mass flow rate through the test section measured by rotameter, $\mathrm{kg\,s^{-1}}$
$\dot{m}''$ = mass flux through the core region, $\mathrm{kg\,s^{-1}\,m^{-2}}$

N = dimensionless time at which steady state has been achieved
Nu = Nusselt number
P = pressure, Pa
P_C = induction coil pitch m
Pr = Prandtl number
$\dot{Q}'''$ = heat generation rate per unit solid volume, W m^{-3}
Re = pore Reynolds number
s = skin heating depth, m
S = specific surface area, m^{-1}
T = temperature (simulation), K
t = time, s
$\hat{t}$ = dimensionless time
ΔT_f = characteristic temperature difference, K
U = core superficial velocity, m s^{-1}
U' = upstream superficial velocity, m s^{-1}
u = interstitial velocity, m s^{-1}
$\hat{u}$ = dimensionless velocity
V = volume, m^3
x = spatial coordinate, m
$\hat{x}$ = dimensionless spatial coordinate
y = radial coordinate from the wall, m
z = dimensionless transformed radial distance from the wall

Greek Symbols

α = governing equation parameter; thermal diffusivity, m^2 s^{-1}
β = governing equation parameter
γ = governing equation parameter
δ = dimensionless fluid temperature response between the inlet and exit of the test section
ϵ = volumetric porosity
θ = dimensionless temperature
τ = characteristic time scale, s
μ = dynamic viscosity, kg m^{-1} s^{-1}
μ_r = relative magnetic permeability of the test section
ρ = density, kg m^{-3}
ρ_R = electrical resistivity of the test section material, Ω m
χ = hydraulic diameter to length ratio

Subscripts and Superscripts

avg = average over space and time
c = core
C = coil
eff = effective
exp = experimental
f = fluid
in = inlet (fluid), initial
lim = limiting
max = maximum
min = minimum
o = mean
out = outlet (fluid)
s = solid
sim = simulated
$\ldots'$ = upstream; overall; or reference quantities
* = experimentally measured value

References

[1] Kays, W. M., and London, A. L., 1950, "Heat Transfer and Flow Friction Characteristics of Some Compact Heat Exchanger Surfaces, Part 1—Test System and Procedure," Trans. ASME, **72**, pp. 1075–1085.
[2] Kays, W. M., and London, A. L., 1984, *Compact Heat Exchangers*, McGraw-Hill, New York.
[3] Hausen, H., 1929, "Theory of Heat Exchange in Regenerators," Zeitschrift fur Angewandte Mathematik und Mechanik, **9**, pp. 173–200.
[4] Schumann, T. E. W., 1929, "Heat Transfer: A Liquid Flowing Through a Porous Prism," J. Franklin Inst., **28**, pp. 405–416.
[5] Locke, G. L., 1950, "Heat Transfer and Flow Friction Characteristics of Porous Solids," Technical Report TR No.10, Stanford University, California.
[6] Kohlmayer, G. F., 1968, "An Indirect Curve Matching Method for Transient Matrix Heat-Transfer Testing in the Low NTU-Range," Int. J. Heat Mass Transfer, **14**, pp. 567–581.
[7] Kohlmayer, G. F., 1968, "Extension of Maximum Slope Method to Arbitrary Upstream Fluid Temperature Change," Trans. ASME J. Heat Transfer, **90**, pp. 130–134.
[8] Rodriguez, J. I., and Mills, A. F., 1990, "Analysis of the Single-Blow Transient Testing Technique for Perforated Plate Heat Exchangers," Int. J. Heat Mass Transfer, **33**(9), pp. 1969–1976.
[9] Liang, C. Y., and Yang, W. J., 1975, "Modified Single-Blow Technique for Performance Evaluation on Heat Transfer Surfaces," J. Heat Transfer, **97**, pp. 16–21.
[10] Stang, J. H., and Bush, J. E., 1974, "The Periodic Method for Testing Compact Heat Exchanger Surfaces," J. Eng. Power, **96A**(2), pp. 87–94.
[11] Younis, L. B., and Viskanta, R., 1993, "Experimental Determination of the Volumetric Heat Transfer Coefficient Between Stream of Air and Ceramic Foam," Int. J. Heat Mass Transfer, **36**(6), pp. 1425–1434.
[12] Nie, X., Besant, R. W., Evitts, R. W., and Bolster, J., 2011, "A New Technique to Determine Convection Coefficients with Flow Through Particle Beds," Trans. ASME J. Heat Transfer, **133**(4), p. 041601.
[13] Jones, S., and Catton, I., 1998, "Non-Intrusive Heat Transfer Coefficient Determination in Highly Porous Metal/Ceramic Foams," HTD-Vol. 361-5, Proceedings of the ASME Heat Transfer Division, ASME, Vol. 5.
[14] Rhee, S. J., 1977, "Natural Convection Heat Transfer in Beds of Inductively Heat Particles," M.S. thesis, University of California, Los Angeles, pp. 23–25.
[15] Somerton, C. W., 1982, "Natural Convection and Boiling in Porous Media," Ph.D. thesis, University of California, Los Angeles, pp. 50–53, 140–142.
[16] Cherng, J. C., 1978, "Effect of Bottom Cooling on Natural Convection in Beds of Inductively Heated Particles," M.S. thesis, University of California, Los Angeles.
[17] Mills, A. F., 1999, *Heat Transfer*, Prentice-Hall, Upper Saddle River, NJ.
[18] Incropera, F. P., Dewitt, D. P., Lavine, A., and Bergman, T. L., 2007, *Fundamentals of Heat and Mass Transfer*, John Wiley & Sons, Hoboken, NJ.
[19] Benenati, R. F., and Brosilow, C. B., 1962, "Void Fraction Distribution in Beds of Spheres," AIChE J. **8**(3), pp. 359–361.
[20] H. Martin, 1978, "Low Peclet Number Particle-to-Fluid Heat and Mass Transfer in Packed Beds," Chem. Eng. Sci., **33**, pp. 913–919.
[21] Achenbach, E., 1995, "Heat and Flow Characteristics of Packed Beds," Exp. Therm. Fluid Sci., **10**, pp. 17–27.
[22] Ziółkowska, I., and Ziółkowski, D., 1988, "Fluid Flow Inside Packed Beds," Chem. Eng. Process, **23**, pp. 137–164.
[23] Schlunder, E. U., 1978, "Transport Phenomena in Packed Bed Reactors," *Chemical Reaction Engineering Reviews-Houston, American Chemical Society Symposium Series*, D, Luss and V. W. Weekman, eds., Vol. 72, pp. 110–161.
[24] Fiers, B., Ferschneider, G., and Maillet, D., 2010, "Reduced Model for Characterization of Solid Wall Effects for Transient Thermal Dispersion in Granular Porous Media," Int. J. Heat Mass Transfer, **53**(25–26), pp. 5962–5975.
[25] Scheidegger, A. E., 1957, *The Physics of Flow through Porous Media*, University Toronto Press.
[26] Travkin, V. S., and Catton, I., 2001, "Transport Phenomena in Heterogeneous Media Based on Volume Averaging Theory," Adv. Heat Transfer, **34**, pp. 1–144.
[27] Viskanta, V., 1995, "Modeling of Transport Phenomena in Porous Media Using a Two-Energy Equation Model," ASME/JSME Thermal Engineering Conference, Vol. 3.
[28] Wakao, N., Kato, K., 1969, "Effective Thermal Conductivity of Packed Beds," J. Chem. Eng. Jpn, **2**(1), pp. 24–33.
[29] Whitaker, S., 1972, "Forced Convection Heat Transfer Correlations for Flow in Pipes, Past Flat Plates, Single Cylinders, Single Spheres, and for Flow in Packed Beds and Tube Bundles," AIChE J., **18**(2), pp. 361–371.
[30] Kar, K. K., and Dybbs, A., 1982, "Internal Heat Transfer Coefficients of Porous Metals," *Heat Transfer in Porous Media*, J. V. Beck, and L. S. Yao, eds., ASME, New York, Vol. 22, pp. 81–91.
[31] Rajkumar, M., 1993, "Theoretical and Experimental Studies of Heat Transfer in Transpired Porous Ceramics," M.S.M.E. thesis, Purdue University, West Lafayette, IN.
[32] Galitseysky, B. M., and Moshaev, A. P., 1993, "Heat Transfer and Hydraulic Resistance in Porous Systems," *Experimental Heat Transfer, Fluid Mechanics and Thermodynamics*, Kelleher M. D., Sreehivasan K. R., Shah R. K. and Toshi Y. eds., pp. 1569–1576.
[33] Kokorev, L. S., Subbotin, V. I., Fedoseev, V. N., Charitonov, V. V., and Vosokobojnikov, V. V., 1987, "The Relationship between the Hydraulic Drag and Heat Transfer Coefficients in Porous Media," High Temperature., **25**, pp. 92–96.
[34] Gortyshov, Y. F., Muravev, G. B., and Nadyrov, I. N., 1987, "Experimental Study of Flow and Heat Exchange in Highly Porous Structures," J. Eng. Phys. Thermophys., **53**(3), pp. 987–990.
[35] Spalding, D. B., Taborek, J., and Armstrong, R.C., 1983, *Heat Exchanger Design Handbook*, Hemisphere Publishing Corporation, New York.
[36] Anzelius, A., 1926, "Uber Erwarmung Vermittels Durchstromender Medien," Z. Angew. Math. Mech. **6**, 291–294